Microwave Journal

mmWave Beamforming in Dynamic, Urban Environments

Kenneth M. O'Hara
Remcom Inc., State College, Pa.

In 5G and 6G, mmWaves bring the promise of new, high bandwidth frequency bands, supporting many of the new concepts envisioned for future applications in wireless communications. Propagation losses and fast fading due to increasingly mobile devices and short wavelengths pose challenges for many of these new concepts. mmWave MIMO beamforming technology can help solve some of these issues but must be able to adapt to dynamic channels as devices move and signals interact with people and vehicles moving through a scene. To evaluate performance, ray tracing simulations can predict the fast fading and Doppler spectra expected in an active urban environment and estimate the impact a dynamic channel has on MIMO beamforming.

To support the demand for significantly higher data rates and an ever-increasing number of connected users, wireless service providers have begun using the large expanse of spectrum available in the mmWave band; however, mmWave propagation presents unique challenges. Principal among these are increased free-space path loss and greater attenuation for diffracted beams when compared to the sub-7 GHz bands. To mitigate the increased path loss, high gain antennas for one or both ends of the link are employed. At the base station, exceptionally high gains are attained with many-element phased arrays forming massive MIMO (mMIMO) links with users. The use of such high gain antennas, in turn, demands that adaptive beam steering be used in mobile scenarios. This introduces challenges of its own.

ADAPTING TO A DYNAMIC CHANNEL

Since the channel is continuously changing, latency between the measurement of channel state information (CSI), e.g., beam selection and/or channel sounding, and use of the adapted beam for data transmission yields a throughput that is degraded relative to that achievable in a static scene. This degradation can be particularly severe for high mobility scenarios and for scenes with obstacles that can dynamically block a link, as shadow fading is particularly sharp for mmWaves. For these reasons, an accurate prediction of link performance in a mobile environment requires knowledge of the time dependent channel and an understanding of relevant latencies.

Beyond the challenges associated with adaptive beamforming, the mmWave channel is also a faster fading channel compared to sub-7 GHz channels because of the shorter wavelength. Thus, the coherence time is shorter, and the corresponding Doppler bandwidth is broader. For the orthogonal frequency division multiplexing (OFDM) waveforms used in 5G New Radio (NR), the increased Doppler bandwidth results in interference between subcarriers yielding further degradation of throughput.

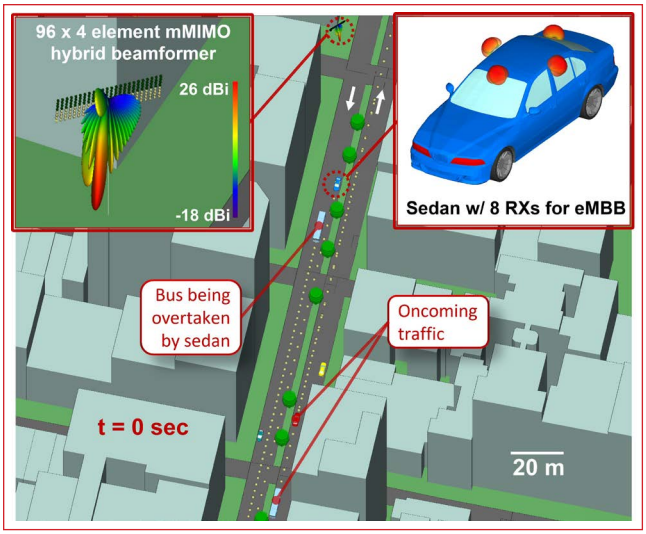

Fig. 1 **mmWave hybrid beamformer transmitting four data streams to a sedan driving in central Manhattan.**

CASE STUDY

To illustrate the impairments due to mobility, consider the use case of providing enhanced mobile broadband (eMBB) service to a moving vehicle in a dense urban environment and in the presence of other moving vehicles. Realistic predictions of the time-varying channels are made using Remcom's Wireless InSite® propagation tool[1] to perform ray tracing simulations over a series of densely-spaced time steps. Simulations show that the vehicle-mounted receivers (Rx) detect fading as the vehicle moves along its route, and illustrate an example of a Doppler spectrum that results from the motion of the vehicle receiving service and other vehicles around it. Next the degradation in the signal-to-interference-plus-noise ratio (SINR) due to latency between measuring and using the CSI for adaptive beamforming is considered. Relative to the case where mobility is ignored, this latency alone provides a degradation of 5 to 8 dB in the SINR for latency parameters suggested by the 5G NR standard.[2-4]

The specific eMBB scenario considered here is the hybrid beamforming of four data streams to a mobile vehicle. This scenario is motivated by a recent 5G NR field trial[5] where a data rate of 11 Gbps was demonstrated across four data streams and 732 MHz of aggregated bandwidth for a vehicle moving at 30 km/h and communicating with hybrid beamforming mMIMO base stations operating at 28 GHz. For an increased speed of 100 km/h, the throughput was reduced to 8 Gbps. Whereas the field trial was conducted in a pristine environment, within the context of our simulations, a similar vehicle-to-network (V2N) interface is deployed but in a dense urban environment and in the presence of additional moving vehicles (see ***Figure 1***).

The sedan which receives the eMBB service is equipped with a total of eight Rxs: two cross-polarized Rxs at each of four locations as shown in the upper right inset. Further, the sedan is equipped with four baseband RF chains so that it can decode four data streams from the four Rxs with the highest signal strength. The 5G Node B (gNB) radio base station is located at the top center of Figure 1 and shown in detail with exaggerated dimensions for visualization in the upper-left inset. The gNB is a 28 GHz hybrid beamformer consisting of four digital baseband RF chains. Each drives a 96-element phased array equipped with an analog beamformer. Each 96-element panel is a rectangular array that spans four elements in the vertical direction and 24 in the horizontal dimension with $\lambda/2$ spacing. The elements themselves are patch antennas with 6 dBi gain. Two panels are co-located but with elements having orthogonal polarizations at ±45 degrees relative to vertical. The second set of two panels are similarly co-located but positioned vertically above the first two-panel set. The four-panel assembly is angled down by 10 degrees to increase coverage to users at street level. Each panel is equipped with an analog beamformer which enables beam steering over 32 angles in the horizontal direction evenly spaced across a 120-degree span. These 32 directed beams are configured in the precoding matrix that can be requested by the user equipment (UE), i.e., the sedan receiving service. One such beam produced by a single panel is shown in the upper-left inset of Figure 1. The total RF power output by the four-panel array is 27 dBm.

Having four digital baseband RF

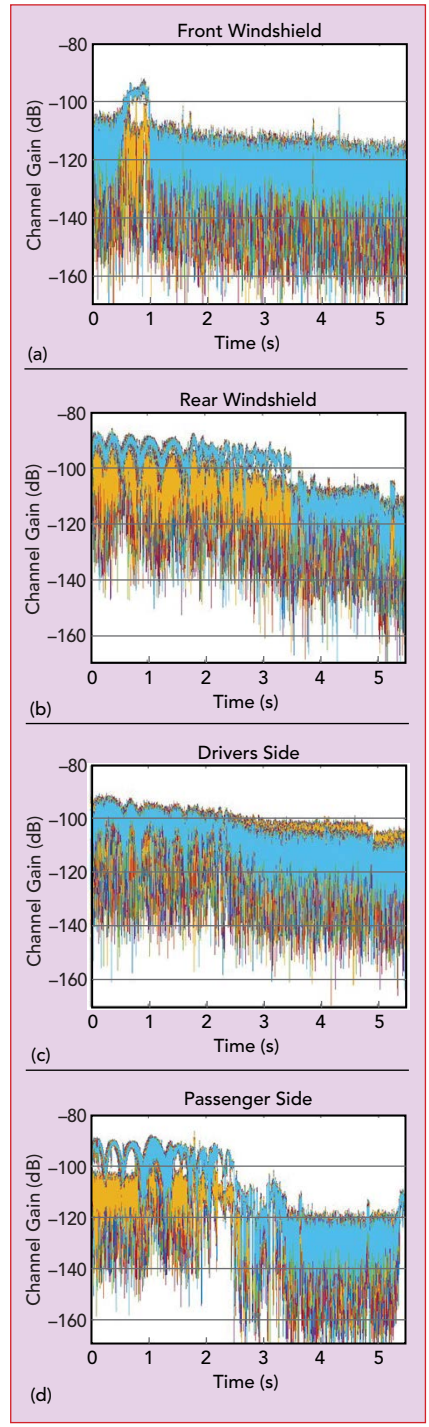

Fig. 2 **Receiver fading at the front windshield (a), rear windshield (b), driver side (c) and passenger side (d) of the moving sedan over 5.5 s.**

chains, the gNB can simultaneously transmit four data streams to the UE. The gNB does so by employing digital beamforming using one beam from each panel selected from the precoding matrix. With these four analog-formed beams, the digital beamformer employs regularized-zero-forcing (RZF)[6] to determine the optimum complex weight coefficients for transmitting each of the four data streams to an individual Rx on the UE, while simultaneously minimizing interference to the other three active Rxs not associated with a given data stream.

The UE travels along Park Avenue at a constant speed of 14.75 m/s. Along the route, it overtakes a bus moving at 7 m/s in the adjacent lane and is proximate to oncoming traffic, a car (14 m/s) and a bus (13 m/s). Figure 1 depicts the scenario at an initial time, t = 0 s, where the yellow dots which extend in front of each moving vehicle denote waypoints at equal time intervals for the given route.

DETERMINISTIC CHANNEL MODEL

Before considering the effects of latency on beamforming, first consider the general characteristics of the fading channels for the scenario described above. Remcom's Wireless InSite is used to evaluate the propagation channels by performing ray tracing for each of the 384 × 8 element pairs between the mMIMO gNB and the UE's Rxs. Ray tracing is performed at each of a dense series of time steps spaced by 2.5 ms over a time interval between t = 0 and 5.5 s.

New mobility features currently under development in the Wireless InSite propagation tool facilitate simulation of the motion of the UE along with other vehicles in the scene so that any geometry that can affect the propagation channel is accurately accounted for at each time step. Ray path trajectories which connect a transmit-receive (Tx-Rx) element pair can include up to six reflections, one diffraction and attenuation by foliage. In addition, diffuse scatter off the terrain, asphalt and nearby buildings is included. Linear interpolation of ray path parameters (e.g., path length, path loss and phase shift) between time steps allows a reliable means to reconstruct ray path properties at arbitrary times. The parameters for each ray path at an arbitrary time can then be used to calculate the complex path gain and, by coherently summing over all complex path gains, the complex channel gain for each Tx-Rx element pair.

FADING AND SHADOWING

These results are used to predict channel fading for each Tx-Rx element pair as a function of time. ***Figure 2*** shows the magnitude of the channel gains over the entire route for each of the 384 mMIMO elements to four representative Rxs on the UE:

Front Windshield (see ***Figure 2a***). For most of the time, this Rx does not have a strong path from any mMIMO element, but typically has a channel gain determined by the sum of many diffuse scatter contributions, which arrive from a multitude of directions. As a result, one observes very fast fading for much of the time with rapid fluctuations in channel gain. There is a period, however, from t ≈ 0.5 to 1.0 s, over which the channel gain is relatively large for the mMIMO elements of one polarization. This is due to a strong reflection off the slow-moving bus that the UE is gaining on which exists over this period, allowing significant power to reach the Rx.

Rear Windshield (see ***Figure 2b***). For this Rx, the characteristics of fading for the first ≈ 3.5 s are notably different from the front windshield Rx, as the gain is significantly increased and has a fading contribution that fluctuates on a slower time scale. This is because a line-of-sight (LOS) and one or more specular rays are incident on this Rx over this period. Beyond 3.5 s they are shadowed by one or both buses.

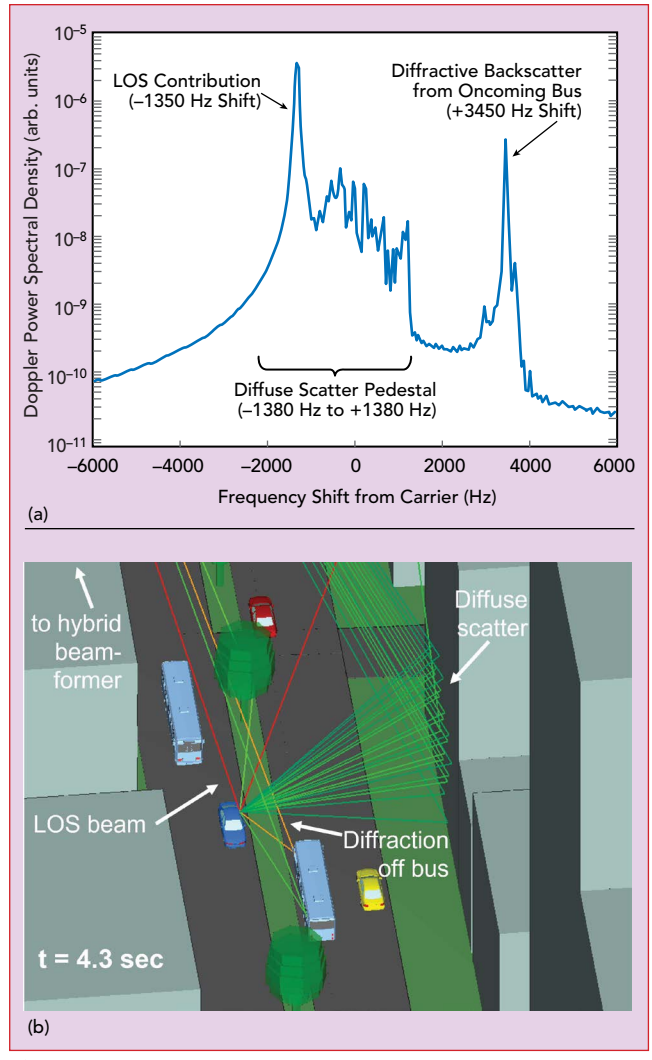

▲ Fig. 3 **Doppler shift at the driver's side receiver (a) showing effects of diffraction from an oncoming bus (b).**

Driver and Passenger Side Rxs (see ***Figures 2c*** and ***d***). These Rxs show similar behavior to the rear window Rx, as they also have a LOS and strong multi-path components reaching the Rxs for the initial portion of the route. The passenger side Rx is abruptly shadowed at t ≈ 2.5 s, at which point the UE is overtaking the bus on its passenger's side.

All Rxs. For all Rxs, a slow fade is observed for short to long timescales due to free-space path loss as the UE recedes from the gNB.

DOPPLER SHIFTS

Another quantity of interest is the distribution of frequency shifts that arise due to the Doppler effect, as such shifts introduce inter-(sub)-carrier-interference (ICI) in an OFDM waveform and thereby degrade the communication link. The power spectral density (PSD) of the Doppler frequency shifts relative to the carrier is given by the PSD of the time dependent complex channel gain over a given interval.

A typical Doppler spectrum is shown in ***Figure 3a*** where the PSD is computed over a 20 ms period at a simulation time of t = 4.3 s. The spectrum shown is the average over all mMIMO elements for a single Rx on the driver's side of the UE. There are several notable features explained with reference to ***Figure 3b***, which shows the 25 highest power (out of 500) ray paths that contribute to the received signal for a representative mMIMO element.

The dominant peak in the Doppler spectrum arises primarily from the LOS ray path, with smaller contributions from somewhat weaker reflected rays. Since the UE is moving almost directly away from the gNB with a speed $|\vec{v}|$= 14.75 m/s, the expected frequency shift for the LOS contribution is close to the maximum shift $\Delta f_{max}=|\vec{v}|/\lambda$ = 1.38 kHz. The observed shift, with a magnitude of 1.35 kHz, is reduced because the velocity of the UE is not directly away from the gNB, and the reflected rays also contribute with somewhat reduced shifts. The negative sign of the shift is expected since the UE is moving away and therefore receives a LOS signal lower in frequency than that of the carrier. This dominant peak sits on top of a broad pedestal, which extends from $-\Delta f_{max}$ to $+\Delta f_{max}$ and results from diffuse scatter contributions to the PSD, which arrive from all directions relative to the velocity, $\vec{v}$, of the UE.

Finally, the isolated peak having a frequency shift of +3.45 kHz results from rays that first travel to the oncoming bus, diffract off the bus and, finally, travel back to the driver's side Rx. The size of this shift is reasonable. With the bus approaching the gNB at a velocity of $\vec{v}_{bus}$, and the UE and bus approaching each other with a relative velocity of $(\vec{v}_{bus} - \vec{v})$, the expected Doppler shift would be $(2\,|\vec{v}_{bus}| + |\vec{v}|)/\lambda$ = 3.8 kHz. Given that these objects are not moving directly toward each other, the reduced shift of 3.45 kHz is expected.

It is notable that this representative Doppler spectrum differs significantly from the often-used statistical model of Clarke[7] and Jakes,[8] which assumes a dense, uniform scattering environment and ignores strong, isolated contributions that arise from LOS or specular ray paths. The Doppler spectra for the deterministic channel simulated here, in contrast, includes contributions from LOS and specular rays which yield the dominant features in the Doppler spectrum, highlighting the value of deterministic ray tracing simulations. Further, though it is beyond the scope of this article, the time dependent ray path parameters provided by these simulations can be used to construct the time dependent channel impulse response (CIR) from which the explicit degradation of the communication link due to ICI can be determined (e.g. Wang et al.,[9] but using a deterministic rather than a statistical CIR).

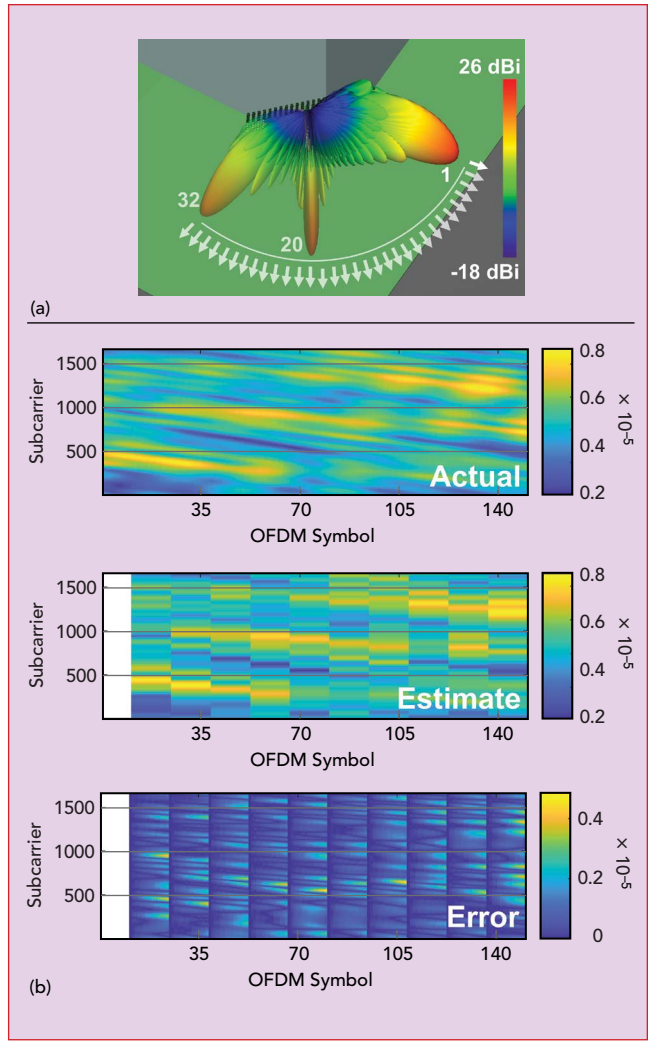

▲ Fig. 4 **Sector scan during a signal synchronization burst (a) with channel estimation based on sounding reference signal (b).**

BEAMFORMING DEGRADATION DUE TO LATENCY

Consider now the SINR attained for four downlink data streams to active Rxs on the UE achieved by digital RZF beamforming using four analog-formed beams, each chosen from the precoding table. Latencies which exist between channel measurement and beamforming degrade performance.

The four active Rxs (out of eight on the UE) and the precoding matrix indices (PMIs) requested by the UE are chosen following a burst of synchronization signal blocks (SSBs) which are part of the 5G NR and can be expected once every 20 ms.[4,10] During a SSB burst, the gNB scans a sector by transmitting 64 SSBs using each of the 32 analog-formed beams for each of two orthogonally polarized panels in succession (see ***Figure 4a***). During the SSB bursts, the UE determines the four Rxs out of eight that have the highest signal strength from one of the 64 SSBs.

Since the UE only has four digital RF chains, two successive SSB bursts are required to determine the four active Rxs. Thus, with a period of 40 ms, the UE chooses an active Rx set and reports to the gNB the four unique

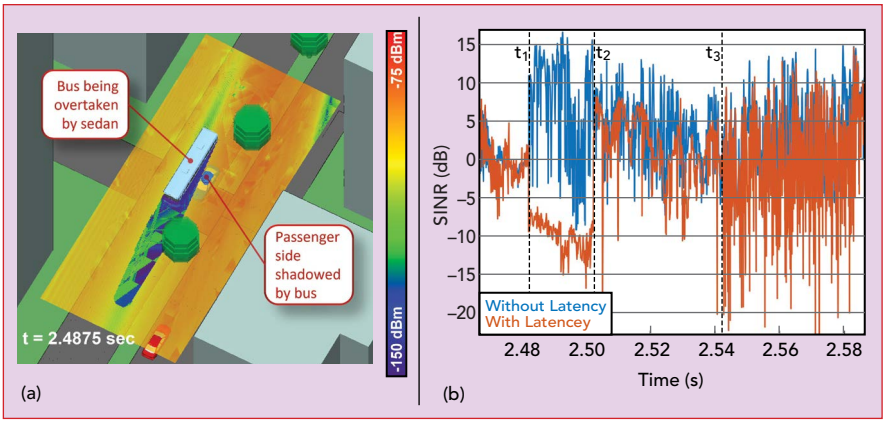

▲ Fig. 5 **Driving scenario (a) with SINR degradation due to latency in the analog beamforming stage (b).**

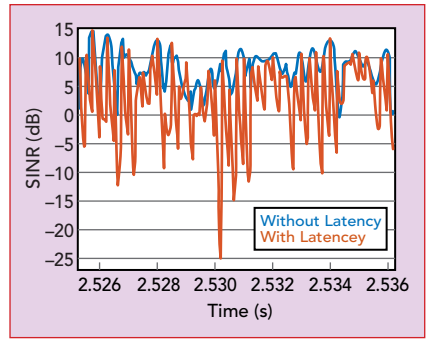

▲ Fig. 6 **SINR degradation from the latency in the digital beamforming stage.**

PMIs which produced the highest signal strengths. These are used to generate four beams for the analog stage of the hybrid beamforming. Next, the CSI required for the digital beamforming stage is obtained from sounding reference signals (SRSs) provided by the UE on uplink (channel reciprocity is assumed). Per the 3GPP specifications,[2] the SRS can be provided as often as once per slot; which, for a 60 kHz subcarrier spacing, is a period of 250 µs.

The latency due to both the analog and digital stages of channel estimation in beamforming degrades performance. For example, in the case of PMI set + Rx set selection, motion of the UE or other vehicles in the scene can result in abrupt shadowing of one or more active Rxs from one or more analog-formed beams. Regardless, the gNB will continue to use this compromised PMI + Rx set for beamforming until another set is chosen at a time up to 40 ms in the future despite the significant reduction in SINR over this period.

In the case of SRS-based channel estimation, discrepancies between the measured and actual CSI grow due to the channel changing continuously between SRS measurements. An example of this is shown in ***Figure 4b*** where the top panel shows the magnitude of the actual channel gain across a ≈ 100 MHz bandwidth (assuming 60 kHz subcarrier spacing) as a function of time. This CSI is sampled and stored by the gNB (middle panel) once per slot where one slot = 14 symbols = 250 µs. Over the period of one slot, the error between the stored and actual CSI grows continuously from zero. Figure 4 shows CSI for a driver's side Rx to a representative mMIMO element over a period of 40 ms starting at t = 2.5 s.

Explicit examples of degraded SINR resulting from each case considered above is readily found in the simulation. For example, ***Figure 5*** shows the SINR (red trace in ***Figure 5b***) for data stream #4 over a period that includes the moment (t_1 = 2.483 s) when the passenger side Rxs become rapidly shadowed by a bus. Prior to this moment, at t_0 = 2.463 s, the PMI/Rx set had been chosen to include a passenger side Rx for stream #4. When this Rx becomes shadowed at t_1, however, the SINR is significantly degraded relative to that which could be achieved if the analog and digital beams were formed based on instantaneous channel measurements (blue trace).

In this case, with latency ignored, the PMI/Rx sets chosen at t_1 switch to using driver's side Rxs for streams #3 and #4, which have direct LOS. In the realistic case, with latency considered, the gNB continues to attempt to form beams to the passenger side Rxs until the PMI/Rx sets are updated after the SSB burst at t_2 = 2.503 s (e.g., Figure 5a shows the gNB's attempt to form a beam to a passenger side Rx at a time between t_1 and t_2 even though it is shadowed). In fact, even at t_2, the updated active Rx set still includes one of the passenger side Rxs, because the signal strength recorded for that Rx was measured during the SSB burst just prior to its being shadowed at t_1. Thus, it is only when the PMI/Rx sets are updated again at t_3 = 2.543 s that both passenger side Rxs become excluded from the active Rx set.

A representative time sequence demonstrating degraded SINR due to latency in SRS-based channel estimation is shown in ***Figure 6***. The red trace shows the SINR for stream #3 associated with an Rx on the driver's side. This SINR varies periodically from a large value immediately after each SRS measurement to a low value just prior to the subsequent SRS measurement. The periodic degradation in SINR results precisely from the difference between the actual CSI and the CSI periodically captured by the gNB as depicted in Figure 4b. For comparison, the blue trace in Figure 6 shows the SINR that would be attained if the gNB used the actual CSI at all times for beamforming (i.e., ignoring latency).

COMPREHENSIVE RESULTS

To gauge the total impact latency has on beamforming for the eMBB scenario considered here, the SINR for the scenario as described above, which includes latencies based on 5G NR standards, is compared to the same scenario but with the effect of latency ignored (i.e., the PMI/Rx set selection is made and current CSI is used at each timestep for beamforming). The SINRs for both scenarios are calculated between t = 22.5 ms and 3.5 s with a 25 µs time step. Beyond the final time of 3.5 s, the UE is strongly shadowed.

A histogram of the results across all four data streams is shown in ***Figure 7a***. The corresponding cumulative distribution functions (CDFs) are shown in ***Figure 7b*** where an additional CDF result is included for a scenario where the

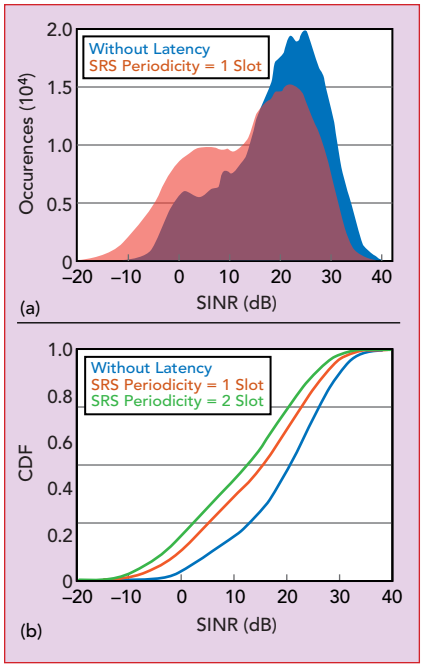

Fig. 7 Effects of latency on beamforming: histogram across four data streams (a) and corresponding CDFs (b).

SRS measurements are made once every two slots. The median SINR is 20.5 dB, 15.4 dB and 12.4 dB for the case which ignores latency and the cases that include all latency effects but use an SRS periodicity of one slot and two slots respectively. Thus, the combined effects of latency, including both PMI/Rx set selection and CSI measurement, act to degrade the median SINR by 5.1 dB when a one slot SRS periodicity is used and 8.1 dB for a two slot SRS periodicity.

CONCLUSION

Accessing the wide bandwidths afforded by mmWaves necessitates the use of adaptive beam steering methods with degraded performance in a mobile environment due to latency. To assess the performance impact for realistic scenarios, an eMBB use case in a dynamic urban scene is employed using ray tracing simulations to provide a time dependent deterministic channel model for analysis.

The impact from latency alone, evaluated here, can be significant, resulting in a 5 to 8 dB loss in SINR for feasible parameters. The quantitative impact of other effects of mobility on the communications link, such as Doppler shifts which introduce ICI, have not been included here and will further degrade performance. All such effects, however, can be calculated deterministically using, as input, time dependent CIRs constructed from the ray tracing simulations. Ray tracing simulations can provide the foundation for the accurate evaluation of link performance in a mobile environment incorporating all effects which act to degrade service quality. ■

References

1. "Wireless InSite 3D Wireless Prediction Software," *Remcom Inc.*, 2021, www.remcom.com/wireless-insite-em-propagation-software.
2. "Physical Channels and Modulation," Release 15, 3GPP TS 38.211, V.15.4.0, January 2019.
3. "Multiplexing Channel Coding," Release 15, 3GPP TS 38.212, V.15.4.0, January 2019.
4. "Physical Layer Procedures for Control," Release 15, 3GPP TS 38.213, V.15.4.0, January 2019.
5. "Success with 5G Communications Using 'Vehicle Glass Mounted Antenna' for 5G Connected Car," *AGC Incorporated and NTT DOCOMO Incorporated*, July 2018, www.agc.com/en/news/detail/1197413_2814.html.
6. C. B. Peel B. M. Hochwald and A. L. Swindlehurst, "A Vector-Perturbation Technique for Near-Capacity Multiantenna Multiuser Communication – Part I: Channel Inversion and Regularization," *IEEE Transactions on Communications*, Vol. 53, No. 1, Jan., 2005, pp. 195–202.
7. R. H. Clarke, "A Statistical Theory of Mobile Radio Reception," *The Bell System Technical Journal*, Vol. 47, No. 6, July-August 1968, pp. 957–1000.
8. W. C. Jakes, "Microwave Mobile Communications," Wiley, New York, 1974.
9. T. Wang, J. G. Proakis, E. Masry and J. R. Zeidler "Performance Degradation of OFDM Systems Due to Doppler Spreading," *IEEE Transactions on Wireless Communications*, Vol. 5, No. 6, June 2006, pp. 1422–1432.
10. "Radio Resource Control Protocol Specification," Release 15, 3GPP TS 38.331, V.15.4.0, January 2019.